8th Pan American Conference for Nondestructive Testing 2025, 9-12.June, 2025 Niagara Falls, Canada

e-Journal of Nondestructive Testing - ISSN 1435-4934 - www.ndt.net

Feasibility Assessment of Guided Wave Generation in Rail Using Electromagnetic Acoustic Transducers for In-Service Inspection

Andrea APPIANI [1], Michele CARBONI [1]

[1] Department of Mechanical Engineering, Politecnico di Milano, Milan, Italy
Phone: +39-02-23998253, Fax +39-02-23998202; e-mail: michele.carboni@polimi.it

Abstract
This study investigates the use of electromagnetic acoustic transducers to generate and detect ultrasonic guided waves from the rail head for in-service rail inspection. Unlike conventional bulk wave methods using rolling search units, this approach aims to overcome limitations like limited coverage, need for contact, and high noise. A pitch-catch configuration is analyzed, with a transmitter and receiver placed at a realistic distance on the rail head. Due to hardware constraints, a specific excitation frequency had to be used in the experiments; numerical simulations were therefore employed to verify the presence of suitable wave modes in its vicinity. Experimental tests then validate the wave propagation in both healthy and artificially defected rails, assessing detectability and the influence of sleeper positioning. Signal comparisons between defect-free and defective cases aim to identify features indicative of structural anomalies.
Keywords: rail, ultrasonic testing, electromagnetic acoustic transducer, ultrasonic guided waves, in-service inspection

1. Introduction

The structural integrity of railway rails is essential to ensuring the safe and efficient operation of both conventional and high-speed rail networks. In-service failures, such as transverse cracks or head checks, can lead to severe disruptions, costly maintenance, or, in worst cases, derailments. For this reason, non-destructive testing (NDT) techniques have become critical tools for the periodic inspection and monitoring of rails in operation. A variety of NDT methods are currently applied to rail infrastructure, including conventional ultrasonic testing, electromagnetic testing such as eddy current testing and alternating current field measurement, magnetic particle inspection, infrared thermography, radiographic testing, and optical techniques such as automatic visual inspection and fiber optic sensing [1]-[5].
Among these, ultrasonic testing remains the primary method for detecting internal defects within the rail section, particularly when implemented by diagnostic trains equipped with rolling search units (RSUs). These systems use piezoelectric transducers embedded in fluid-filled rolling wheels to introduce bulk waves into the rail from the running surface [6], [7]. Despite their widespread use, RSUs suffer from several limitations. First, effective wave transmission requires physical contact and a coupling medium between the transducer and the rail, which introduces complexity, sensitivity loss, and maintenance issues. Second, inspection is limited by the need for a clear line of sight between the transducer and the potential defect: this constrains the ability to inspect critical zones such as the web and the foot of the rail [8].
To address these challenges, research has increasingly turned to non-contact ultrasonic methods, including, in a few cases, those based on electromagnetic acoustic transducers (EMATs). EMATs can generate and detect ultrasonic waves in conductive materials without the need for coupling media, offering advantages such as reduced sensitivity to surface conditions and the ability to operate in harsh environments or at high speeds [9]-[11]. In the context of rail inspection, EMATs have been primarily explored for the generation of surface and guided waves (e.g., Rayleigh and shear horizontal modes), especially for defect detection in the rail head [12]-[17].
However, current EMAT applications have mostly been limited to localized inspections or to excitation modes that do not sufficiently excite the entire rail cross-section. Moreover, studies

 https://doi.org/10.58286/31367

investigating the feasibility of detecting defects in deeper regions such as the web or foot while operating from the rail head remain scarce [18]-[20].
In this context, the present research explores the use of guided ultrasonic waves generated and detected by EMATs placed on the rail head in a pitch-catch configuration, with the specific aim of exciting wave modes capable of inspecting the entire rail section. This approach could enable efficient, non-contact, in-motion diagnostics of otherwise hard-to-access rail regions, opening new perspectives for full-section rail inspection from diagnostic trains.
The work is organized as follows: Section 2 describes the numerical analyses focused on evaluating the natural modes of a rail chunk of proper dimensions in the surroundings of the bandwidth considered for experiments; in Section 3 the experimental campaign to assess the onset of guided waves is reported, analyzing different configurations in terms of relative positioning between the required sensors as well as across different points of the rail sections, investigating both an intact and defective portions of rail. Eventually, in Section 4, conclusions are drawn and potential future developments discussed.

2. Numerical analysis

A key aspect in the development of guided wave monitoring systems is the definition of dispersion curves for specific geometries. A widely used method relies on Finite Element analysis combined with an eigensolver, where the waveguide model is constrained to allow only in-plane motion. The computed natural frequencies and mode shapes are used to derive phase and group velocities [21].
In this study, dispersion analysis was performed using ABAQUS 16.1 and its Lanczos eigensolver. The model reproduced a 1762 mm segment of 60E1 rail, imposed by the mounting configuration on a diagnostic bogie studied and developed elsewhere [20] and was meshed with 42064 C3D20R elements using a 10 mm seed size. Material properties were assumed homogeneous, isotropic and liner-elastic: Young's modulus 206 GPa, Poisson's ratio 0.3, and density 7800 kg/m³ [22].
Although guided wave inspections often use lower frequencies (~ 100 kHz), this analysis focused around 250 kHz to match the instrumentation bandwidth. Numerical simulations identified several wave modes with selective activation of specific rail regions, shown in Figure 1 (a) to (d), as also observed in previous studies [23]. While such selectivity is beneficial in permanent installations, enhancing defect localization, our system relies on a moving setup witch excitation and reception limited to the rail head. To avoid loss of coverage, a mode exciting the full cross-section was needed. A suitable mode was found at 249 921 Hz and selected for experimental validation. Its normalized displacement is shown in Figure 1 (d).

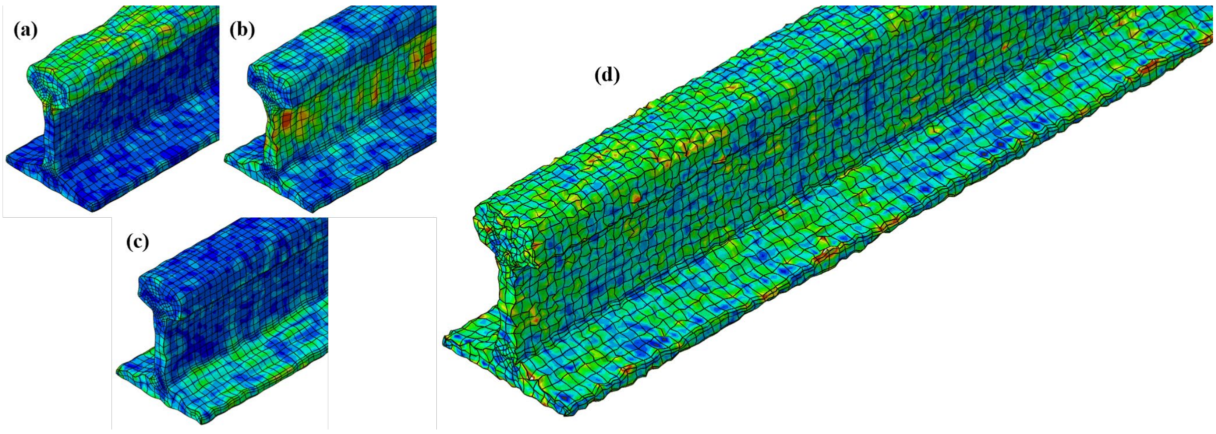

Figure 1 – Selected natural mode exciting the whole rail section

3. Experimental analysis

Following the numerical analyses, an experimental campaign was conducted to validate the results.

3.1 Experimental setup and procedure

The EMAT equipment employed throughout all the tests consisted of a PowerBox H by Innerspec Technologies, Inc., to which two EMAT sensors were connected, identified by producer's codes 274A0169 (transmitter) and 274A0170 (receiver) [24]. From a constructive point of view, the two sensors are identical, featuring a racetrack-shaped coil of 25.4 by 25.4 mm^2 embedded in a permanent magnet, to which it is permanently attached. Pictures of the sensors and the experimental setup are reported in Figure 2 (a) and (b), respectively.

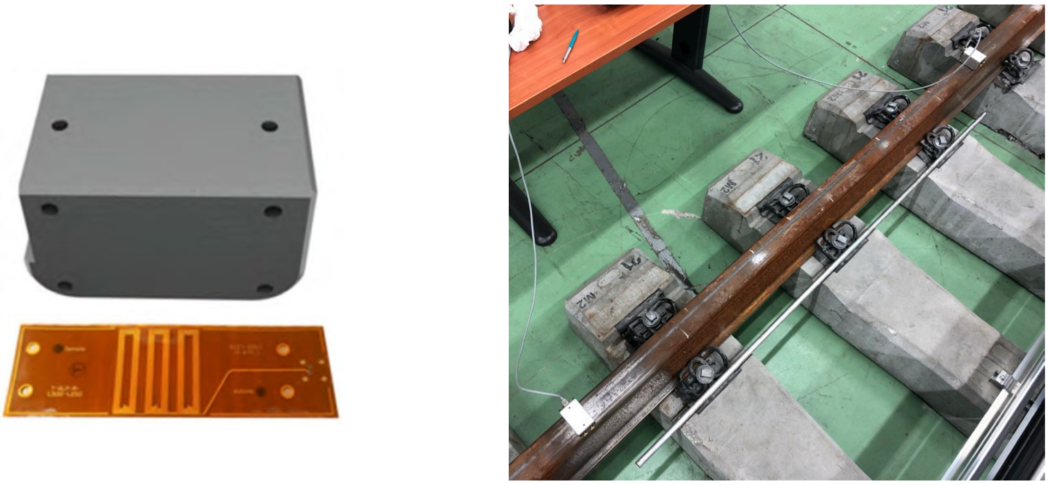

(a) (b)

Figure 2 – (a) EMAT sensor; (b) experimental setup

The goal of this activity was to verify the effective onset of a guided wave mode capable of activating the whole rail section while acting on the rail head only. The transmitter was fixed in a centered position on the rail head and the receiver positioned at a constant distance of 1762 mm, as anticipated, and sequentially moved across ten predefined locations around the rail cross-section including the head, web, and foot regions. The specific locations and nomenclature of the receiver's position are shown in Figure 3.

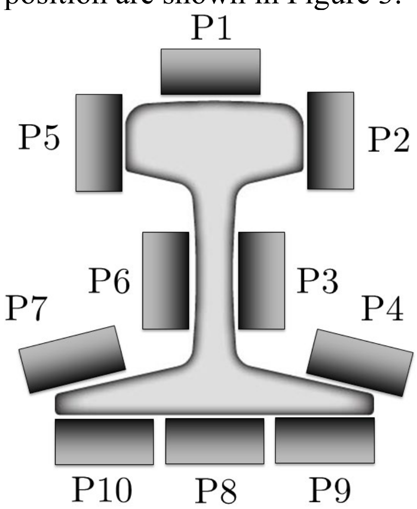

Figure 3 – Positions of the receiver around the inspected section

Moreover, three experimental configurations, shown in Figure 4, were adopted to evaluate the influence of the rail fastening system (sleeper, pad, and clips) on wave propagation, as well:

- C1 – transmitter midway between two sleepers;
- C2 – transmitter at the start of a sleeper;
- C3 – symmetric configuration, with transmitter and receiver equidistant from the midpoint between two sleepers.

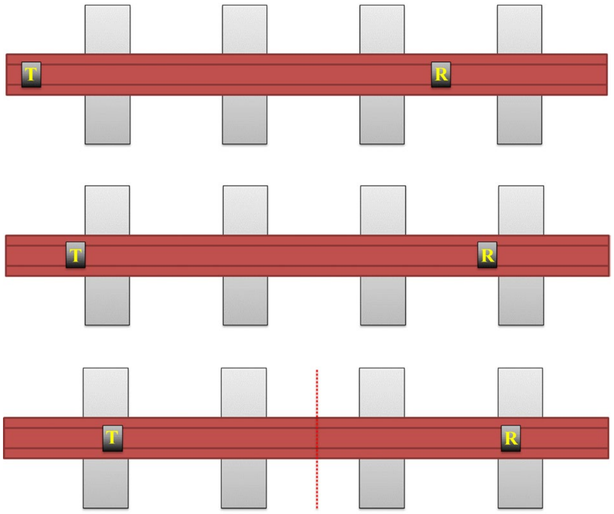

Figure 4 – Configurations tested for intact rail: C1 (top), C2 (mid), C3 (bottom). T indicates the transmitter, R the receiver

A time window of 750 µs and a sampling frequency of 10 MHz were chosen to capture the full wave packet while maintaining a manageable record length. To account for the amplitude variability across positions, a gain calibration procedure was applied: the signal acquired in position P1 was recorded using a fixed gain of 25 dB and used as a reference. For the remaining positions, the gain was individually adjusted so that the rectified echo amplitude, averaged within a time gate (480 – 720 µs), matched the reference level. This allowed for a more meaningful comparison of wave propagation across the section.
The same procedure was repeated on a rail segment containing a manufactured defect, consisting in a cut interesting the whole foot region of the section. Three configurations were considered:

- RC – receiver close to the defect (1/4 of the sensor distance);
- RF – transmitter close to the defect (reciprocal to RC);
- S – symmetric placement with the defect midway between transmitter and receiver.

3.2 Intact rail

The EMAT system proved capable of generating guided waves that propagate throughout the entire rail cross-section. While signal amplitudes were naturally higher near the excitation point (e.g., P1 – P3), lower values were recorded in the foot area (P4, P8 – P10), especially in configurations where the presence of the sleepers restricted optimal sensor placement. A summary of the test results is reported in Table 1. Nevertheless, through gain normalization, usable signals were recovered in all positions. The influence of sleeper-related configurations was minimal in the head and web, but more pronounced in the foot, where structural constraints and mode sensitivity introduced larger amplitude variations: this is reported in Figure 5, where the signals (in normalized amplitude) shown in every subfigure are associated with a specific receiver position and the three different setup configurations are compared.

Table 1 – Reference value and gains registered for the intact rail

	Ref [%]	P2 [dB]	P3 [dB]	P4 [dB]	P5 [dB]	P6 [dB]	P7 [dB]	P8 [dB]	P9 [dB]	P10 [dB]
C1	24	35.5	40.5	42	34.5	34.5	44	36.5	33.5	35.5
C2	22.5	35.5	39	42	36.5	35.5	46	38	33	36
C3	20	35.5	37.5	38	36	34.5	43.5	30.5	31	31.5

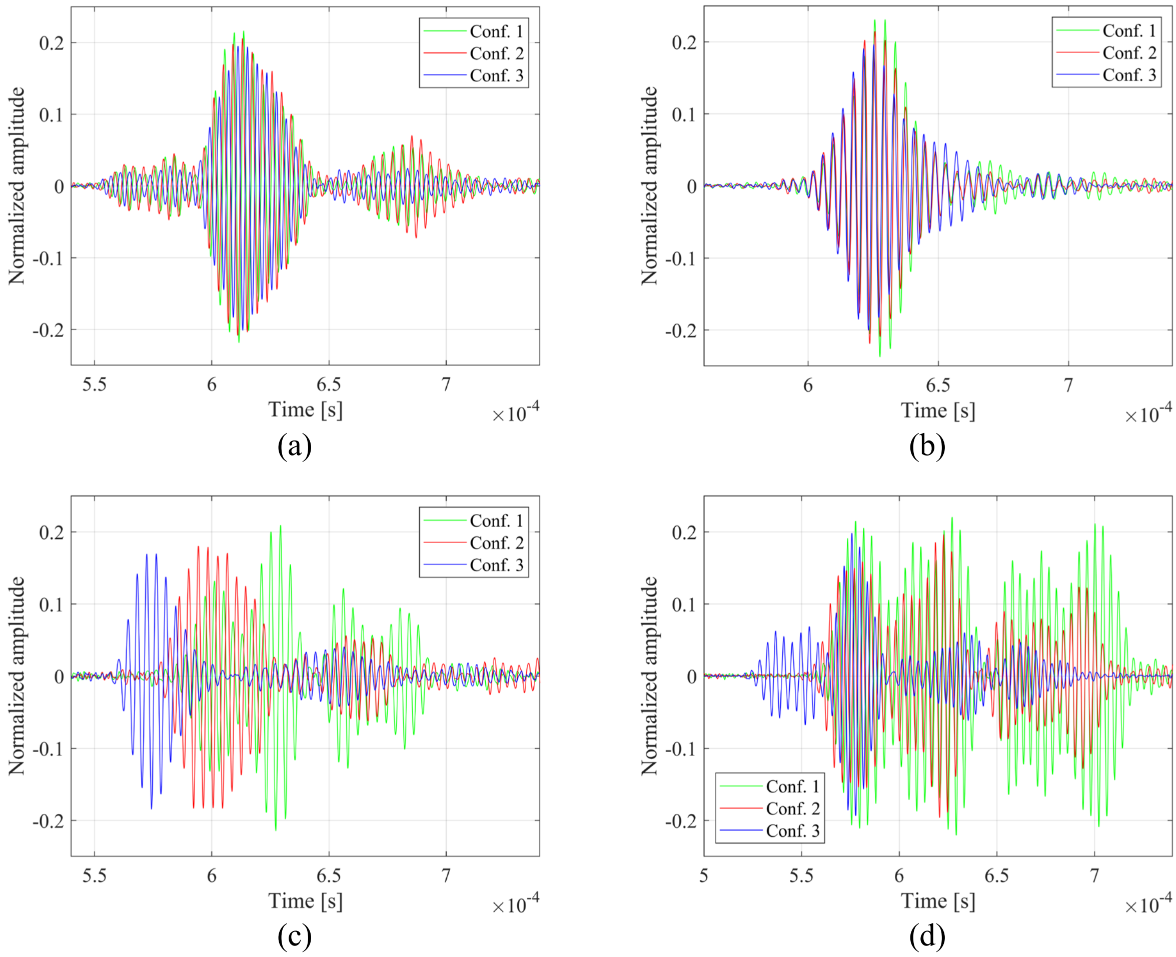

Figure 5 – Wave comparison for the intact rail. (a) P2; (b) P6; (c) P4; (d) P8

3.3 Defective rail

The presence of a defect led to notable variations in both amplitude and waveform, even in the upper cross-sectional positions. The reference values and gains for the defective rail are reported in Table 2, while the registered signals for the same positions as the intact rail are show in Figure 6, in normalized amplitude. In particular, measurements at P8 showed strong sensitivity to the location of the defect relative to the sensors, confirming its effect on wave propagation. This influence was configuration-dependent, with RC, RF, and S setups producing markedly different signals even across multiple positions.

Table 2 – Reference values and gains registered for the defective rail

	Ref [%]	P2 [dB]	P3 [dB]	P4 [dB]	P5 [dB]	P6 [dB]	P7 [dB]	P8 [dB]	P9 [dB]	P10 [dB]
RC	25	38	40	44.5	37	36	46	36.5	38	40
RF	26	36.5	43	45.5	35	42	45	37.5	31.5	33.5
S	23	37	39	42	38.5	37.5	44	38.5	40.5	41

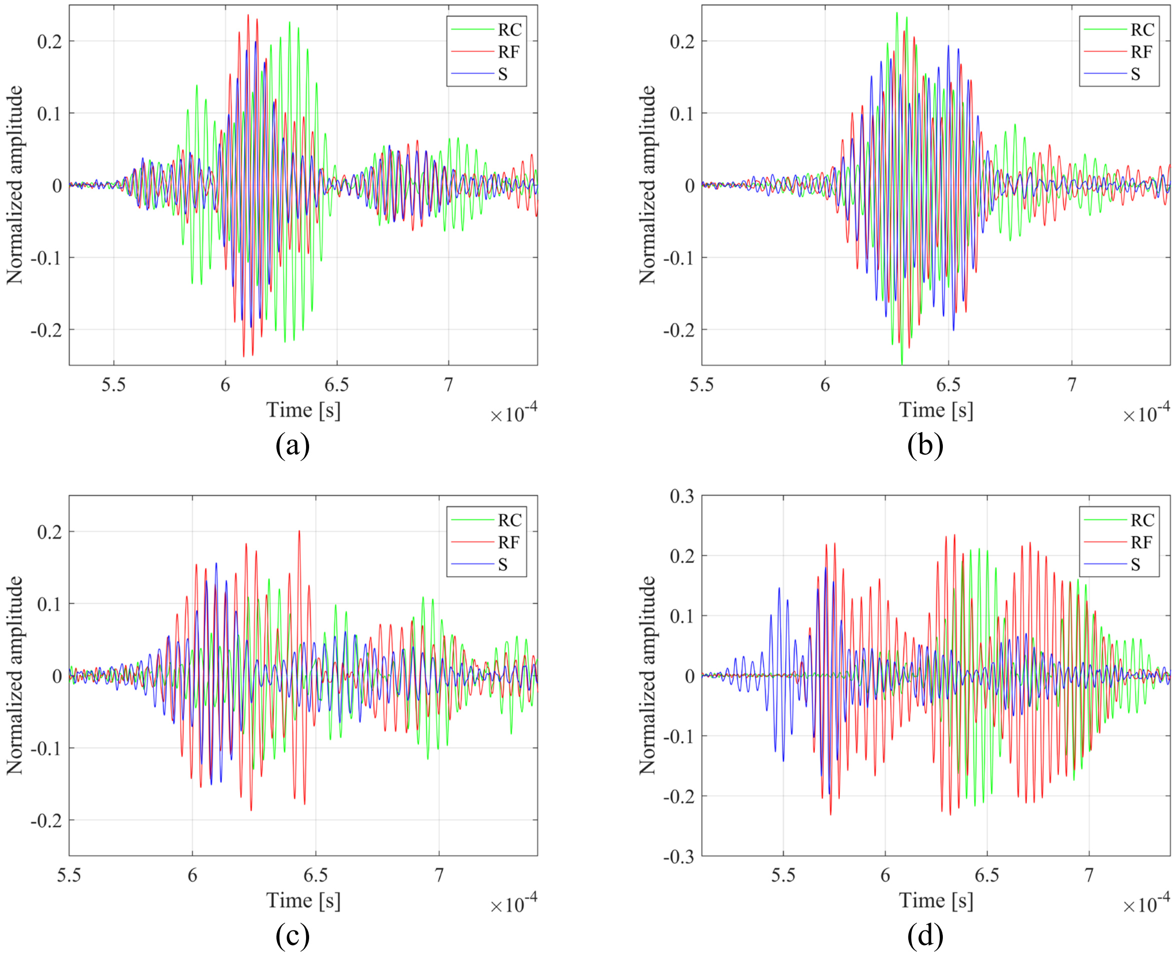

Figure 6 – Wave comparison for the defective rail. (a) P2; (b) P6; (c) P4; (d) P8

3.4 Rail head waves comparison

Finally, since in-motion inspections can only rely on sensors positioned on the rail head, the comparison focuses on signals acquired in position P1. In particular, Configuration 3 of the intact rail is compared to the symmetric configuration of the defective one, where both transmitter and receiver are placed at the same relative distance and position. This comparison, presented in Figure 7, shows that the wave packet reaches the receiver at the same time in both cases, but with visible differences in amplitude and waveform. In general, the signal acquired from the defective rail exhibits a broader wave packet, especially in its later components. Notably, a small tail of oscillations appears in the final part of the wave in the defective rail, between 660 and 680 µs, as highlighted in the figure, suggesting that the presence of the defect affects the wave propagation.

4. Conclusions

This work demonstrated the feasibility of using EMAT-generated guided waves for rail inspection, focusing on modes capable of exciting the entire cross-section. Numerical and experimental analyses confirmed the possibility of detecting guided waves across the profile, even in the presence of defects. Although differences between intact and defective rails are more pronounced in less accessible positions, only the rail head is viable for in-motion inspection. Results show that even from this location, meaningful variations in waveform and amplitude can be detected, supporting the method's practical applicability. Future work will further explore in greater detail these signal differences, investigate lift-off operation, and assess system performance under dynamic conditions.

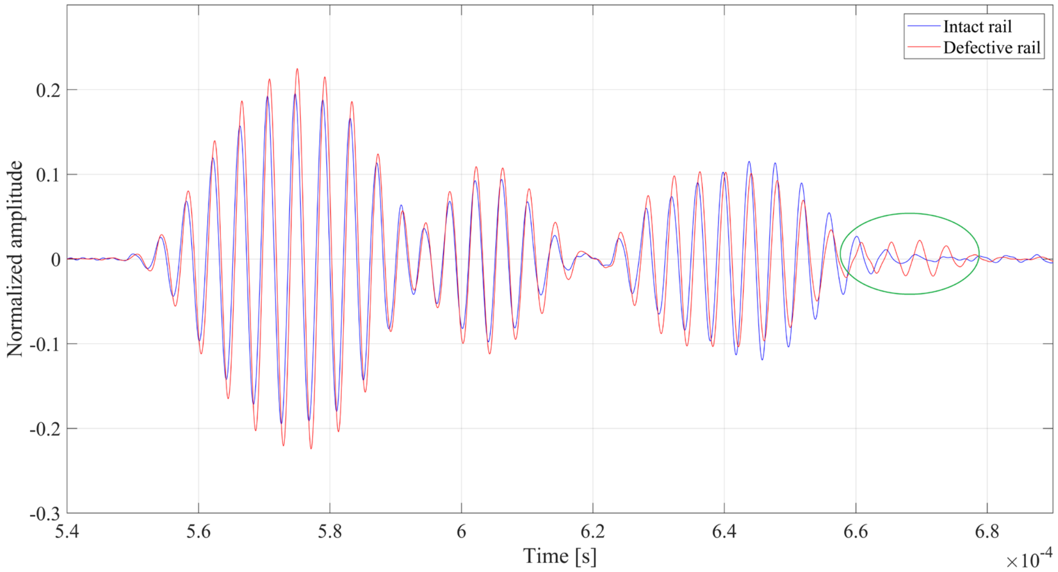

Figure 7 – Comparison between signals at P1, intact vs. defective rail

References

1. Papaelias, M.Ph., Roberts, C., Davis, C.L. A review on non-destructive evaluation of rails: state-of-the-art and future development. Proceedings of the Institution of Mechanical Engineers, Part F: Journal of Rail and Rapid Transit. 2008;222(4):367-384. doi: 10.1243/09544097JRRT209.
2. Alahakoon, S., Sun, Y. Q., Spiryagin, M., and Cole, C. Rail Flaw Detection Technologies for Safer, Reliable Transportation: A Review. ASME. J. Dyn. Sys., Meas., Control. February 2018; 140(2): 020801. https://doi.org/10.1115/1.4037295.
3. R. Clark. Rail flaw detection: overview and needs for future developments. NDT & E International, vol. 37, no. 2, pp. 111–118, Mar. 2004, doi: 10.1016/J.NDTEINT.2003.06.002.
4. Mićić, M., Brajović, L., Lazarević, L. and Popović, Z. Inspection of RCF rail defects – Review of NDT methods. Mech Sys Sign Proc, 182, 2023, 109568. doi: https://doi.org/10.1016/j.ymssp.2022.109568.
5. Xiong, L., Jing, G., Wang, J., Liu, X. and Zhang, Y. Detection of Rail Defects Using NDT Methods. Sensors, 23, 2023, 4627. doi: https://doi.org/10.3390/s23104627.
6. EN 16729. Railway applications – Infrastructure – Non-destructive testing on rails in track – Part 1: Requirements for ultrasonic inspection and evaluation principles. CEN, Brussels, 2016.
7. Poudel, A., Lindeman, B., Wilson, R. Current Practices of Rail Inspection Using Ultrasonic Methods: A Review. Mater Eval 77, 870–883, 2019.
8. Wang, H., Li, Y., Wang, F., Zhang, G., Xie, J., & Zhang, S. Development of an ultrasonic system for nondestructively detecting flaws in the rail foot of in-service railway, Measurement, 2025, 117289. doi: 10.1016/j.measurement.2025.117289.
9. Hirao, M., Ogi, H. Electromagnetic Acoustic Transducers, 2nd edition, Springer-Verlag, 2017.

10. Frost, H. M. Electromagnetic–ultrasound transducers: Principles, practice, and applications, in Physical Acoustics, vol. 14, Academic Press, 1979, pp. 179-275. doi: 10.1016/B978-0-12-571914-7.50008-X.
11. Thompson, R. B. Physical principles of measurements with EMAT transducers, in Physical Acoustics, vol. 19, Academic Press, 1990, pp. 157-200. doi: 10.1016/B978-0-12-413519-0.50008-3.
12. Rose, J. L., Cho, Y. A guided wave approach to defect detection under shelling in rail. NDT & E International, vol. 42, no. 3, pp. 174–180, Apr. 2009, doi: 10.1016/J.NDTEINT.2008.09.013.
13. Rose, J. L., Avioli, M. J., Mudge, P., Sanderson, R. Guided wave inspection potential of defects in rail. NDT & E International, vol. 37, no. 2, pp. 153–161, Mar. 2004, doi: 10.1016/J.NDTEINT.2003.04.001.
14. Fan, Y., Dixon, S., Edwards, R. S., Jian, X. Ultrasonic surface wave propagation and interaction with surface defects on rail track head. NDT & E International, vol. 40, no. 6, pp. 471–477, Sep. 2007, doi: 10.1016/J.NDTEINT.2007.01.008.
15. Hu, S., Shi, W., Lu, C., Chen, Y., Chen, G., & Shen, G. Rapid detection of cracks in the rail foot by ultrasonic B-scan imaging using a shear horizontal guided wave electromagnetic acoustic transducer, Ndt & E International, vol. 120, 2021, 102437. doi: 10.1016/j.ndteint.2021.102437.
16. Petcher, P. A., Potter, M. D. G., & Dixon, S. A new electromagnetic acoustic transducer (EMAT) design for operation on rail, Ndt & E International, vol. 65, 2014, pp. 1-7. doi: 10.1016/j.ndteint.2014.02.004.
17. European Commission, RIFLEX (Rail inspection by Flexible Electromagnetic Acoustic Transducer), Final Report Summary, 2016.
18. Xue, Z., Xu, Y., Hu, M., & Li, S. Systematic review: Ultrasonic technology for detecting rail defects, Construction and Building Materials, vol. 368, 2023, 130409. doi: 10.1016/j.conbuildmat.2023.130409.
19. Ge, H., Chua Kim Huat, D., Koh, C. G., Dai, G., & Yu, Y. Guided wave–based rail flaw detection technologies: State-of-the-art review, Structural Health Monitoring, vol. 21, no. 3, 2022, pp. 1287-1308. doi: 10.1177/14759217221102952
20. Appiani A., Carboni M. A feasibility study on in-service non-destructive inspection of railway rails by an ultrasonic technique based on travelling electromagnetic acoustic transducers. Accepted for publication in Railway Engineering Science (JMTR), 2025.
21. Masmoudi M., Yaacoubi S., Koabaz M., Akrout M., Skaiky A. On the use of ultrasonic guided waves for the health monitoring of rails. Proceedings of the Institution of Mechanical Engineers Part F Journal of Rail and Rapid Transit 236:469–489, 2021. doi: 10.1177/09544097211025898
22. EN 13674-1. Railway applications - Track - Rail - Part 1: Vignole railway rails 46 kg/m and above. CEN, Brussels, 2002).
23. Bartoli I., Di Scalea F.L., Fateh M., Viola E. Modeling guided wave propagation with application to the long-range defect detection in railroad tracks. NDT & E International 38:325–334, 2004. doi: 10.1016/j.ndteint.2004.10.008
24. Innerspec Technology, Inc. Standard Sensors & Accessories for EMAT Applications. Rev. T-SA-C18, 2018.